Part IV: Sensor Applications

Chapter 8

Polarimetric distributed feedback fiber laser sensor for simultaneous strain and temperature measurements[1]

Abstract — We report the application of a dual polarization distributed feedback (DFB) fiber laser as a strain and temperature sensor. By measurement of the absolute wavelength of one polarization as well as the polarization beat frequency, strain and temperature were determined simultaneously. The sensor has an accuracy of $\pm 3\mu\varepsilon$ and $\pm 0.04^{\circ}$C. Self-heating of the DFB fiber laser as a function of pump power was measured with this sensor.

OCIS codes: 060.2370, 280.3420.

8.1 Introduction

Fiber-optic Bragg grating sensors are a promising device for measuring strain and temperature in a variety of structures. Bragg gratings are written noninvasively into optical fibers [1, 2] making the sensor head very compact. The measurands are wavelength encoded, offering high accuracy and wavelength division multiplexing capabilities of several sensors. However, as the grating wavelength is a function of strain and temperature, the elimination or compensation of this strain-temperature cross-sensitivity has become of great technological interest in recent years.

[1] This chapter is a re-edited version of [O. Hadeler, E. Rønnekleiv, M. Ibsen and R. I. Laming, "Polarimetric fiber distributed feedback laser sensor for simultaneous strain and temperature measurements", Appl. Opt. Vol.38, pp. 1953–1959 (1999)].

Several techniques have been developed and demonstrated to separate the strain and temperature response of fiber Bragg grating sensors. These include compensating temperature drifts by employing two independent sensors, [3] the first one subject to strain and temperature and the second one subject to temperature only. Careful packaging and positioning of the sensors is required for ensuring that the temperature difference between the two sensors remains constant and that the second sensor does not experience any strain. A more compact design can be achieved by use of a single Bragg grating sensor capable of measuring strain and temperature simultaneously. By superimposing two gratings at different wavelengths, such a sensor has been demonstrated [4] making use of the different strain and temperature responses at the two grating wavelengths. The measurement errors were ± 10 $\mu\varepsilon$ and ± 5 °C. Although such a sensor needs two light sources at widely separated wavelengths, Sudo et al. [5] have reported a sensor with a Bragg grating written into birefringent fiber where the grating wavelengths of the two orthogonal polarizations responded differently to strain and temperature. The maximum measurement errors of that polarimetric sensor were ± 20 $\mu\varepsilon$ and ± 2 °C. Alternatively, the thermal response of a grating strain sensor can be canceled by use of a chirped grating in a tapered fiber [6]. However, the elimination of the temperature response might limit the practicality of this strain sensor for structural monitoring because it is impossible to discriminate between mechanically and thermally induced expansion.

A common disadvantage of the above-mentioned passive fiber Bragg grating sensors is that only a small fraction of the spectrally broadband light incident on a narrow-band grating is reflected. This limits the signal-to-noise ratio and therefore the resolution of the sensor. In general, active fiber grating sensors, i.e., sensors where gratings form part of a fiber laser, offer a higher accuracy than passive Bragg grating sensors. The laser intensity is concentrated in a spectral band that is several orders of magnitude narrower than the bandwidth of a passive grating. The laser cavities of distributed Bragg reflection (DBR) fiber lasers are formed by either a broadband mirror and a grating or two gratings at the same wavelength. Typical DBR fiber laser are between a few centimeters and several meters long. Melle et al. [7] reported a DBR fiber laser strain sensor with a resolution of ± 5.4 $\mu\varepsilon$, limited by the electrical noise of the interrogation system. However, in this case, the sensor resolution potentially suffers from mode hopping of these highly multimoded lasers caused by nonuniform environmental changes along the cavity length [7, 8]. Multiplexing of as many as three DBR fiber laser sensors was demonstrated with negligible cross talk between the sensors in [9].

A DBR fiber laser may operate in orthogonal polarization modes if birefringent fiber or birefringent gratings are used in the laser cavity. For lasers with

a sufficiently small birefringence, the beat frequency between the two polarization modes can be measured with a commercial rf spectrum analyzer. External perturbations such as strain and temperature change the birefringence [10] and therefore the polarization beat frequency. Kim et al. [10] demonstrated a polarimetric fiber laser sensor for measuring either strain or temperature. Because of its multimode operation, the rf spectrum exhibited a number of beat frequencies between different longitudinal and polarization modes. The accuracy of the sensor was limited by the broad linewidth of the polarization beatsignal ($\sim$ 1.2 MHz). A DBR fiber laser that was lasing only in two orthogonal polarization modes was demonstrated by Ball et al. [12]. The linewidth of the polarization beat signal was less than 2.5 kHz. Compared with multimode lasers, signal processing becomes much simpler as only one polarization beat frequency is present. Also, the narrow linewidth of the polarization beat signal leads to a higher measurement resolution.

For single-mode operation, DBR fiber lasers must not be longer than a few centimeters and the grating bandwidth has to be below -0.2 nm. The short length usually limits the pump absorption and therefore the output power. Distributed feedback (DFB) fiber lasers are an alternative to DBR fiber lasers with the advantage that they consist of only one grating written into rare-earth-doped fiber. They offer single-mode operation without mode hopping and kilohertz linewidth [13]. With a grating length of -50 mm, DFB fiber lasers are very compact. Furthermore, as most of the laser intensity is concentrated in the center of the grating, the sensitive region is only $\sim$5-10 mm long, [14] making it ideal for point sensing. Multiplexing of five DFB fiber lasers has been demonstrated [15], but only few investigations into lasing stability and sensor accuracy have been carried out. In low birefringent fiber a DFB fiber laser can operate on two orthogonal polarization modes with a ftequency separation between the two modes sufficiently small so that the polarization beat signal can be measured very accurately with a commercial rf spectrum analyser. A birefringent DFB fiber laser operating stably in two polarization modes was employed in [16] as a polarimetric sensor for separately measuring lateral forces and temperature.

In this paper, we demonstrate a similar polarimetric DFB fiber laser sensor for strain and temperature measurements. By measuring both the polarization beat frequency and the absolute wavelength of one polarization, we determined both measurands simultaneously.

8.2 Theory

The wavelengths of the two orthogonal polarization modes of a DFB fiber laser are given by

$$\lambda_{x,y} = 2n_{x,y}\Lambda, \tag{8.1}$$

where $\lambda_{x,y}$ denotes the wavelength of the two orthogonally polarized laser modes, $n_{x,y}$ are the refractive indices of the fiber, and Λ is the grating pitch. For a low birefringent fiber with $n_x \approx n_y \approx n$, the polarization beat frequency becomes

$$\Delta\nu = cB/\left(2n^2\Lambda\right) \tag{8.2}$$

where $B = n_x - n_y$ is the birefringence and c is the velocity of light. Generally, the strain and temperature dependence of $\lambda_{x,y}$ is given by

$$\delta\lambda_{x,y}/\lambda_{x,y} = (1 - p_e)\ \delta\varepsilon|_{\varepsilon=const} + (\alpha + \xi)\ \delta T|_{\varepsilon=const}, \tag{8.3}$$

where p_ε is the strain-optic coefficient, α is the linear thermal expansion coefficient, and ξ is the thermooptic coefficient. Typical values for silica fiber quoted in the literature are $p_\varepsilon = -0.22$, $n_x = 1.46$, $\alpha \approx 0.5 \times 10^{-6}\ \mathrm{K}^{-1}$, and $\xi \approx -8.5 \times 10^{-6}\ \mathrm{K}^{-1}$ [16, 17].

Asymmetrical transverse stress introduces birefringence in the fiber. This stress can build up in noncircular symmetric fibers during fabrication owing to the different thermal contraction of core and cladding. For temperatures below $-350\ ^\circ\mathrm{C}$, the birefringence reduces linearly with increasing temperature as the glass softens.[10]. Theoretical and experimental research [18] has shown that the birefringence is also strain dependent. Both Ball et.al. [10] and Huang et.al. [18] have shown that the strain and temperature dependence of the birefringence is caused by a complex interplay between fiber asynimetries and the different mechanical and thermal properties of the core and cladding. However, the theory proposed [18] is not detailed enough to describe exactly the strain dependence of the birefringence in fibers in which core and cladding have different mechanical properties. Leaving the exact birefringence mechanisms aside, it follows from Eq. (8.2) that $\Delta\nu$ of a birefringent DFB fiber laser changes with strain and temperature according to

$$\begin{aligned}\frac{\delta(\Delta\nu)}{\Delta\nu} &= \left[\frac{1}{B}\frac{dB}{d\varepsilon} - (1 + 2p_\varepsilon)\right]\delta\varepsilon|_{T=const} \\ &\quad + \left[\frac{1}{B}\frac{dB}{dT} - (\alpha + 2\xi)\right]\delta T|_{\varepsilon=const}\end{aligned} \tag{8.4}$$

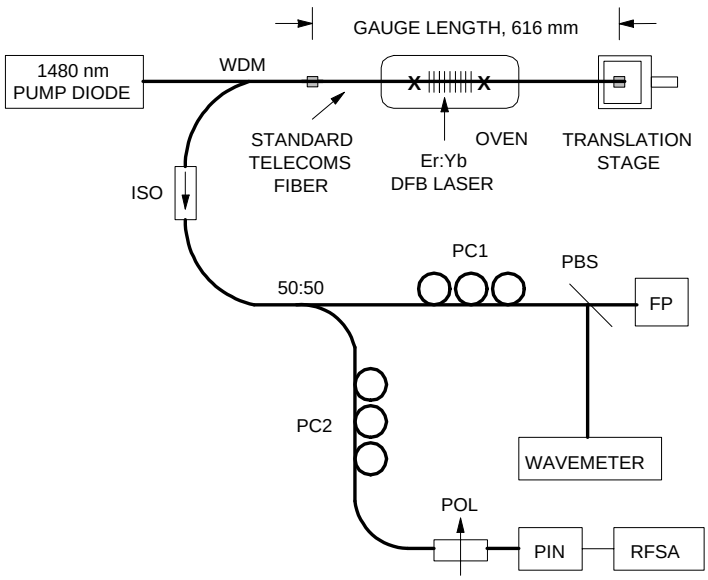

Figure 8.1. Experimental arrangement: WDM, wavelength division multiplexer; ISO, isolator; 50:50, coupler; PC1 and PC2, polarization controllers; PBS, polarizing beam splitter; POL, polarizer; FP, Fabry-Perot spectrometer; PIN, photodiode; RFSA, rf spectrum analyzer.

The responses $\delta\lambda_{x,y}$ and $\delta(\Delta\nu)$ of the DFB fiber laser to strain and temperature [Eqs. (8.3) and (8.4)] can be written in matrix form as

$$\begin{aligned} \begin{bmatrix} \delta\lambda_{x,y} \\ \delta\Delta\nu \end{bmatrix} &= \begin{bmatrix} k_{11} & k_{12} \\ k_{21} & k_{22} \end{bmatrix} \begin{bmatrix} \delta\varepsilon \\ \delta T \end{bmatrix} \\ &= \mathbf{K} \begin{bmatrix} \delta\varepsilon \\ \delta T \end{bmatrix} \end{aligned} \tag{8.5}$$

For a well-conditioned matrix $\mathbf{K}$, i.e., $\det \mathbf{K} \neq 0$, Eq. (8.5) can be inverted. Strain and temperature can then be determined simultaneously by measurement of either $\delta\lambda_x$ or $\delta\lambda_y$ and $\delta\Delta\nu$.

8.3 Experimental Arrangement

The experimental arrangement is shown in Fig. 8.1. A 45 mm long DFB fiber laser was written in an uncoated fiber consisting of an Er^{3+}:Yb^{3+}-doped silica core, a B-Ge-doped silica photosensitive ring around the core, and a silica cladding. The grating coupling coefficient was $\kappa \approx 230\ \mathrm{m}^{-1}$, and the grating phase shift was positioned asymmetrically 20 mm away from the pump input end. The laser operated near $\lambda = 1550$ nm. Standard telecommunication fiber

was spliced to both sides of the laser, approximately 5 mm away from the grating ends. With cyanoacrylate used to bond the coated telecommunication fiber to a fixed metal post and a manual translation stage, the gauge length of the strain sensor was defined. Each bonded region was 10-15 mm long. The gauge length was $l_g = 616$ mm. An oven, consisting of a 150 mm $\times$ 15 mm $\times$ 15 mm aluminium block and a Peltier element, was used to heat the DFB fiber laser. A duct (3 mm $\times$ 3 mm) along the longitudinal axis of the aluminium block accommodated the DFB fiber laser. Care was taken so that the laser did not touch the aluminium block, preventing unwanted strain caused by friction. Furthermore, twist in the fiber was avoided so that additional birefringence was not introduced. The temperature of the aluminium block was regulated with a commercial temperature controller. The thermistor of the control loop was placed -10 mm away from the edge of the Peltier element. The real temperature of the aluminium block was measured with a thermocouple next to the thermistor. The thermocouple had a resolution of ± 0.1 °C, and the temperature controller kept the temperature of the oven to within this resolution. The oven was isolated by 5-15-mm-thick polystyrene. The thermal expansion of the fiber was constrained by the two fixing points of the fiber. Therefore temperature changes of the fiber section in the oven induced thennal stress along the whole length of fiber. The stress related strain was $l_h \alpha \delta T \,/\, l_g$, where l_h is the length of the fiber section in the oven.

The DFB fiber laser was pumped by a 1480-nm diode laser and gave an output power of 430 μW for 82 mW of pump power. The output of the DFB fiber laser was split into two arms by a 50:50 coupler. One arm was used to measure the wavelength $\lambda_{x,y}$ of one polarization with a wavemeter. The polarization controller PC1 was used to align the polarization axes of the laser output parallel to the axes of a fiber-pigtailed polarizing beam splitter (PBS) so that only the x polarization (labeling of the polarization axes is arbitrarily) was incident on the wavemeter. The alignment of the polarization axes was monitored at the second output of the PBS with a scanning Fabry-Perot spectrum analyzer with a free spectral range of 6 GHz and a resolution of 1.2 MHz. The polarization controller PC1 was adjusted until the signal from the x polarization vanished on the Fabry-Perot trace. Measuring $\delta\lambda_{x,y}$ of only one polarization leads to a greater accuracy than measuring the change of the mean wavelength of both polarizations. The latter method could suffer from relative intensity fluctuations between the two polarization modes. As external perturbations of the lead fiber change the polarization state at the input of the PBS, active polarization control or the use of polarization- maintaining fiber should be considered. At the other output of the coupler, the two polarization modes were mixed in a polarizer. The resulting beat signal was detected with a photodiode and the frequency measured with an rf spectrum analyzer. A

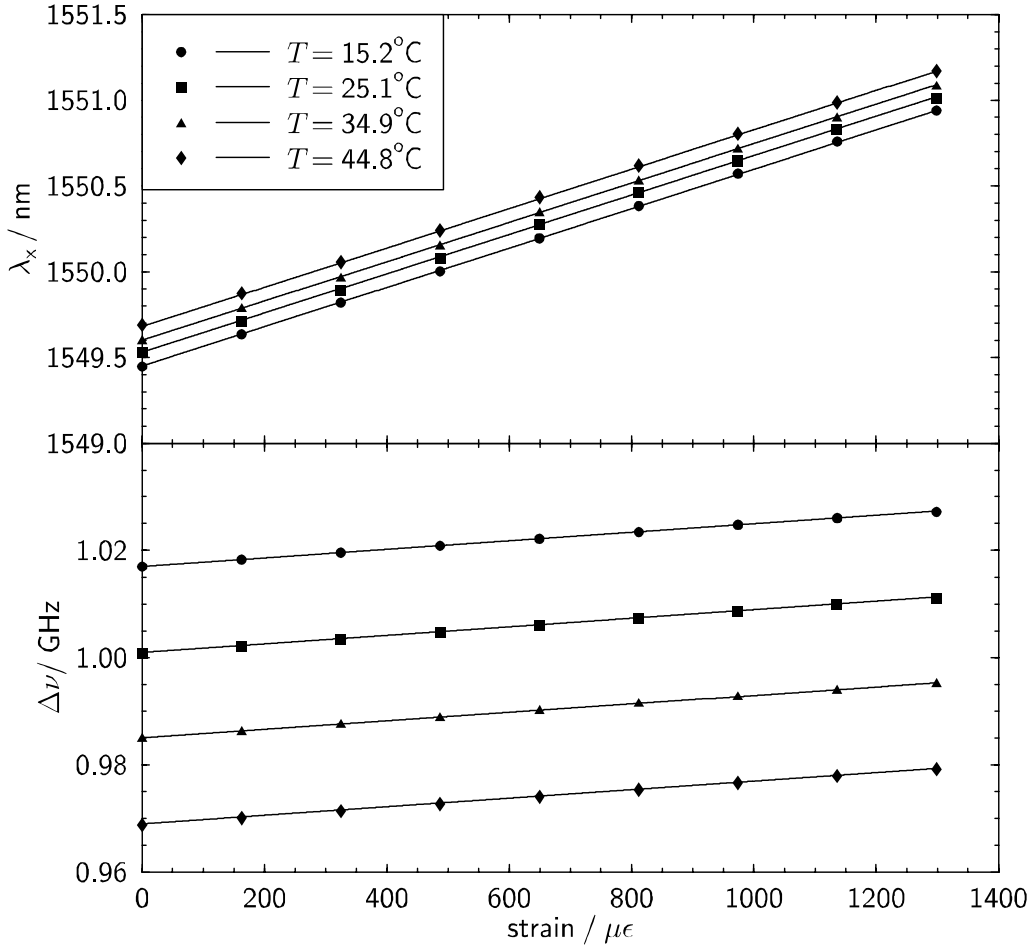

Figure 8.2. Wavelength of x-polarization and polarization beat frequency as a function of strain.

polarization controller (PC2) was used to optimize the signal amplitude on the rf spectrum analyzer.

8.4 Results

The wavelength λ_x of the unstrained DFB fiber laser at room temperature was measured to be 1549.5 nm whilst the polarization beat frequency was $\Delta\nu \sim 1$ GHz with a linewidth of ~ 10 kHz. Inserting $\Delta\nu$, $\lambda_x \approx 2n\Lambda$, and $n = 1.46$ into Eq. (8.2) leads to a birefringence of $B \approx 7.5 \times 10^{-6}$. This birefringence is a combination of the intrinsic fiber birefringence and the birefringence induced by the inscription of the DFB grating. The polarization beat frequency of our DFB fiber laser is approximately 2.3 times bigger than in a previous experiment

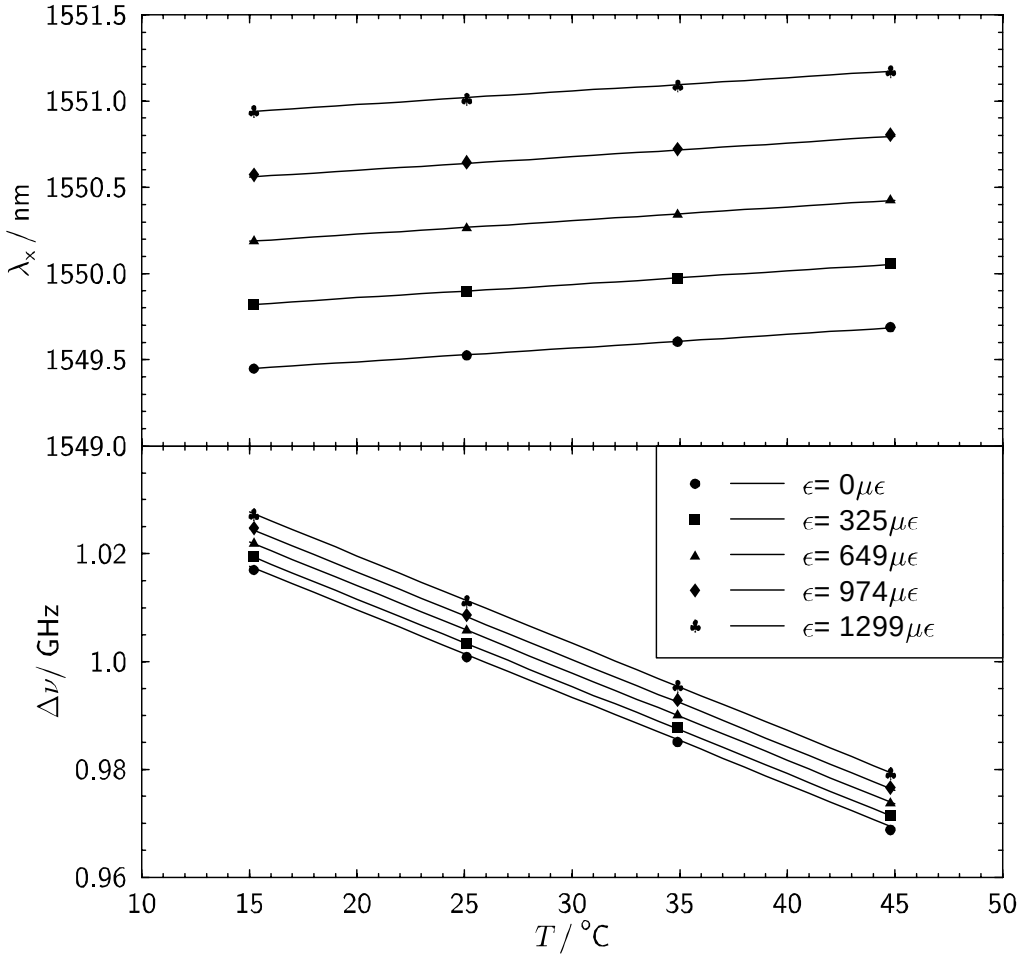

Figure 8.3. Wavelength of x-polarization and polarization beat frequency as a function of temperature. Data of only five strain levels is shown for clarity of the graph.

[16]. This can be attributed to the different fibers used for the two lasers as the grating writing process was essentially the same.

The sensor was calibrated by measurement of λ_x and $\Delta\nu$ at four different temperatures with nine strain levels each. The standard deviation of each measurement was estimated to be $\sigma(\lambda_x) \approx \pm 1$ pm and $\sigma(\Delta\nu) \approx \pm 10$ kHz. The results are shown in Figs. 8.2 and 8.3. Two planes, $\lambda_x(\varepsilon, T)$ and $\Delta\nu(\varepsilon, T)$, were fitted to the data, yielding the following regression coefficients and their

standard deviation:

$$\begin{aligned} k_{11} &= (1.147 \pm 0.002)\ \text{pm}/\mu\varepsilon, \\ k_{12} &= (7.946 \pm 0.065)\ \text{pm}/^{\circ}\text{C}, \\ k_{21} &= (7.946 \pm 0.043)\ \text{kHz}/\mu\varepsilon, \\ k_{22} &= (-1.623 \pm 0.002)\ \text{MHz}/^{\circ}\text{C}. \end{aligned}$$

Note that the numerical equality of k_{12} and k_{21} is pure coincidence.

The analysis of the residuals showed that the deviations of the wavelength measurements from the fitted straight line arose mainly from an uneven motion of the translation stage, which defined the strain. This limits the accuracy of the regression coefficients k_{11} and k_{12}. The resolution ($\pm 0.1^{\circ}$C) of the thermocouple used to measure the oven temperature corresponds to $\delta\Delta\nu = \pm 162$ kHz. The residuals of the beat frequency measurements and the resulting standard deviation of the regression coefficients k_{21} and k_{22} are due mainly to this limited resolution of the temperature measurement. The analysis of the residuals showed no sign of nonlinear strain or temperature response of the sensor. Therefore it can be concluded that any cross-sensitivity between strain and temperature is negligible. Combination of the calibration errors, i.e., the errors of $\mathbf{K}^{-1}$, and the accuracies of the wavelength and polarization beat frequency measurements, $\sigma(\lambda_x)$ and $\sigma(\Delta\nu)$, yields, for this strain and temperature sensor, an accuracy of ± 3 $\mu\varepsilon$ and ± 0.04 °C. The reproducibility of the strain measurements was ± 2.5 $\mu\varepsilon$, which is in agreement with the position reproducibility of the translation stage. Although the telecommunication fiber was coated, no slipping or creep of the fiber was observed. However, at higher strain levels or over longer periods, slipping and creep are potential problems that one can solve by choosing appropriate glues and by using either uncoated fiber or harder coatings. The thermal stress induced by the rise of the fiber temperature from room temperature (25 °C) to 45 °C led to a strain of -2.4 $\mu\varepsilon$, which lies within the accuracy of the sensor. A possible calibration error of the thermometer is not included in the above stated accuracy of the sensor. The resolution of this strain and temperature sensor is limited by the accuracy of the wavelength and the beat frequency measurements. The accuracy of the wavelength measurement is practically limited by the wavemeter used, in this case ± 0.1 pm. The accuracy of the beat frequency measurement is limited by the linewidth of the beat signal, which, in turn, depends on the linewidth of the DFB fiber laser.

The strain dependence $\delta\lambda_x/\lambda_x = k_{11} \times \delta\varepsilon/\lambda_x = 0.74\delta\varepsilon$ is in good agreement with theoretical predictions from Eq. (8.3) of $\delta\lambda_x/\lambda_x = 0.78\delta\varepsilon$. The temperatare dependence $\delta\lambda_x/\lambda_x = k_{12} \times \delta T/\lambda_x = 5.1 \times 10^{-6}K^{-1}$ is smaller than $8.5 \times 10^{-6}K^{-1}$, the value commonly quoted for silica fiber in the literature. This discrepancy probably arises from the rare-earth doping of the fiber, as the

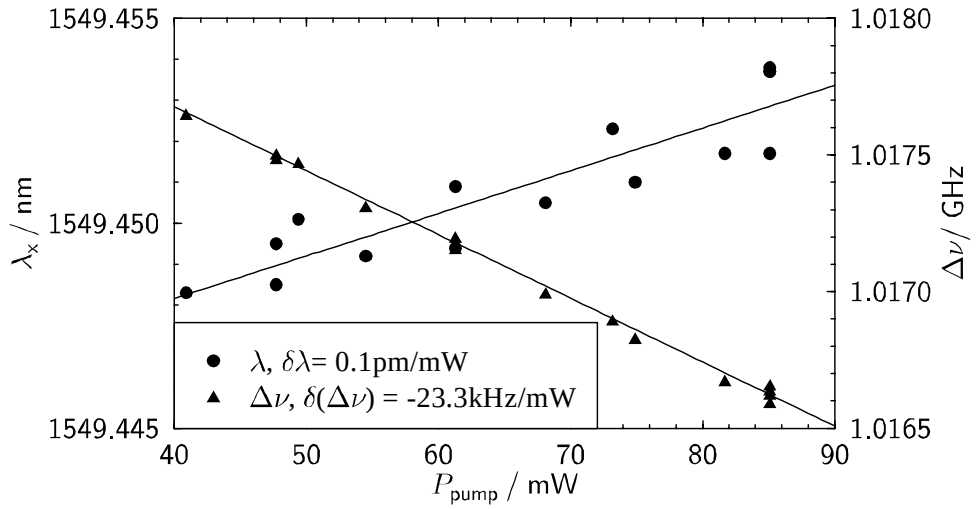

Figure 8.4. Wavelength of x-polarization and polarization beat frequency as a function of pump power at 1480 nm.

value is similar to $4.9 \times 10^{-6} K^{-1}$, which is calculated from the results published by Kringlebotn et.al. in [16]. From the beat frequency measurement $\Delta\nu$, it can be concluded that the birefringence increases with strain. Additional asymmetric stress is probably induced in the strained fiber owing to different mechanical properties of the core, the B-Ge-doped ring, and the cladding. The decrease of $\Delta\nu$ with increasing temperature is expected from theory. The slope $\delta\Delta\nu/\delta T$ depends on the actual thermal properties of the fiber used.

Self-heating of the DFB fiber laser sensor, which is a function of pump power, is a potential source of error. Since the laser intensity is concentrated in the center of the grating and decreases exponentially toward the ends [14], the temperature varies accordingly. Measuring λ_x and $\Delta\nu$ yields a weighted mean or an effective temperature of the DFB fiber laser. While the unstrained fiber was in free air in the oven, the pump power was increased from 40 to 85 mW. Figure 8.4 shows λ_x and $\Delta\nu$ as a function of pump power. The data points lie within the aforementioned accuracy. Fitting two straight lines to the data and using the calibration constants k_{12} and k_{22} reveals that the effective temperature increased by 0.014 ± 0.001 °C/mW. So that the aforementioned accuracy of ±0.04 °C is not exceeded, the pump power must not vary by more than ±3 mW. Although the output power of commercial pump lasers can easily be stabilized to within this limit, variable losses in the lead fiber could potentially cause larger variations. Further investigations on how the pump and lasing intensifies heat the fiber will be carried out in a separate experiment.

8.5 Conclusion

In conclusion, we have demonstrated an active polarimetric strain and temperature sensor based on a birefringent DFB fiber laser. The achieved accuracy of simultaneous measurements of strain and temperature was ± 3 $\mu\varepsilon$ and ± 0.04 °C, respectively. This accuracy was limited by the equipment used to calibrate the sensor, so an improved accuracy should be obtainable. No cross-sensitivity between strain and temperature was observed; the sensor responded linearly to both measurands. The DFB fiber laser operated robustly in two linear polarizations, and it is hoped that multiplexing of several such devices will lead to simple, easy to install, and reliable fiber sensor networks. For industrial applications the sensor can potentially be protected by, e.g., tubes of ~ 50 mm length and ~ 1 mm diameter. Mass fabrication of DFB fiber lasers would result in a low-cost sensor head. The expensive parts of the sensor, the pump laser, and the signal processing unit could be shared between several sensor networks. The use of a digital ftequency counter or a voltage-controlled oscillator locked to the polarization beat frequency would reduce the costs of the signal processing unit. Self-heating of the fiber laser as a function of pump power has also been measured. Pump power fluctuations that could be caused by variable losses in the lead fiber should be kept below ± 3 mW so that the previously mentioned accuracy of the temperature measurements is not exceeded.

8.6 Acknowledgement

O. Hadeler acknowledges the support through a Co-operative Award in Science and Engineering, award from BICC Cables Limited, and the useful discussions with the staff at BICC in Helsby, United Kingdom. The Optoelectronies Research Centre is an interdisciplinary research center funded by the United Kingdom Engineering and Physical Science Research Council.

References

[1] G. Meltz, W. W. Morey, and W. H. Glenn, "Formation of Bragg gratings in optical fibers by a transverse holographic method," Opt. Lett. **14**, 823-825 (1989).

[2] K. O. Hill, B. Malo, F. Bilodeau, D. C. Johnson, and J. Albert, "Bragg gratings fabricated in monomode photosensitive optical fiber by UV exposure through a phase mask," Appl. Phys. Lett. **62**, 1035-1037 (1993).

[3] A. D. Kersey, T. A. Berkoff, and W. W. Morey, "Fiber-optic Bragg grating strain sensor with drift-compensated high-resolution interferometric wavelength-shift detection," Opt. Lett. **18**, 72-74 (1993).

[4] M. G. Xu, J. L. Archambault, L. Reekie, and J. P. Dakin, "Discrimination between strain and temperature effects using dual-wavelength fibre grating sensors," Electron. Lett. **30**, 1085-1087 (1994).

[5] M. Sudo, M. Nakai, K Himeno, S. Suzaki, A. Wada, and R. Yamauchi, "Simultaneous measurement of temperature and strain using PANDA fiber grating," in *Optical Fiber Sensors*, Vol. 16 of 1997 OSA Technical Digest Series (Optical Society of America, Washington, D.C., 1997), pp. 170-173.

[6] M. G. Xu, L. Dong, L. Reekie, J. A. Tucknott, and J. L. Cruz, "Temperature-independent strain sensor using a chirped Bragg grating in a tapered optical fibre," Electron. Lett. **31**, 823-825 (1995).

[7] S. M. Melle, A. T. Alavie, S. Karr, T. Coroy, K Liu, and R. M. Measures, "A Bragg grating-tuned fiber laser strain sensor system," IEEE Photonies Technol. Lett. **5**, 263-266 (1993).

[8] G. A. Ball, W. W. Morey, and P. K Cheo, "Single- and multi- point fiber-laser sensors," IEEE Photonies Technol. Lett. **5**, 267-270 (1993).

[9] A. T. Alavie, S. E. Karr, A. Othonos, and R. M. Measures, "A multiplexed Bragg grating fiber laser sensor system," IEEE Photonies Technol. Lett. **5**, 1112-1114 (1993).

[10] S. C. Rashleigh, "Origins and control of polarization effects in single-mode fibers," J. Lightwave Technol. **LT-1**, 312-331 (1983).

[11] H. K Kim, S. K. Kim, and B. Y. Kim, "Polarization control of polarimetric fiber-laser sensors," Opt. Lett. **18**, 1465-1467 (1993).

[12] G. A. Ball, G. Meltz, and W. W. Morey, "Polarimetric heterodyning Bragg-grating fiber-laser sensor," Opt. Lett. **18**, 1976-1978 (1993).

[13] J. T. Kringlebotn, J. L. Archambault, L. Reekie, and D. N. Payne, "Er^{3+}:Yb^{3+}-codoped fiber distributed-feedback laser," Opt. Lett. **19**, 2101-2103 (1994).

[14] E. Rønnekleiv, M. Ibsen, M. N. Zervas, and R. I. Laniing, "Characterization of intensity distribution in symmetric and asymmetric fiber DFB lasers," in *Conference on Lasers and Electro-Optics*, Vol. 6 of 1998 OSA Technical Digest Series (Optical Society of America, Washington, D.C., 1998), p. 80.

[15] J. Hübner, P. Varming, and M. Kristensen, "Five wavelength DFB fibre laser source for WDM systems," Electron. Lett. **33**, 139–140 (1997).

[16] J. T. Kringlebotn, W. H. Loh, and R. I. Laming, "Polarimetric Er^{3+}-doped fiber distributed-feedback laser sensor for differential pressure and force measurements," Opt. Lett. **21**, 1869-1871 (1996).

[17] H. Singh and J. S. Sirkis, "Simultaneously measuring temperature and strain using optical fiber microcavities," J. Lightwave Technol. **15**, 647-653 (1997).

[18] S.-Y. Huang, J. N. Blake, and B. Y. Kim, "Perturbation effects on mode propagation in highly elliptical core two-mode fibers," J. Lightwave Technol. **8**, 23-33 (1990).

Chapter 9

Intrinsic Distributed Feedback Fibre Laser High Frequency Hydrophone[1]

Abstract — We demonstrate for the first time a distributed feedback fibre laser used as a hydrophone for acoustic frequencies ranging from 0.1 to 1MHz.

9.1 Introduction

Fibre optic interferometric hydrophones have been under development for more than 20 years as an alternative to conventional piezoelectric based hydrophones, and are attractive due to light weight, multiplexing capabilities, and high resolution, making them attractive for hydrophone arrays. Interferometric sensors are based on coils of optical fibre with dimensions mainly limited by the minimum coiling diameter, which is typically 15-20 mm. Smaller sensor dimensions are normally required for high frequency (>100 kHz) acoustic sensing to avoid extremely directive sensors. Also operation in space-restricted areas will require small sensor dimensions.

Distributed Bragg reflector (DBR) fibre laser sensors with interferometric readout have been demonstrated for high resolution strain measurements [1]. DBR lasers are based on one fiber Bragg grating (FBG) reflector at each end of an erbium-doped fibre. They are susceptible to mode-hopping and typically will have effective sensor lengths of several centimetres, which may be too

[1]This chapter contains a re-edited version of the submitted manuscript [D. Thingbø, E. Rønnekleiv and J. T. Kringlebotn "Intrinsic Distributed Feedback Fibre Laser High Frequency Hydrophone", submitted to the Topical Meeting on Bragg Gratings, Photosensitivity, and Poling in Glass Waveguides, to be held in Florida, USA, 1999]

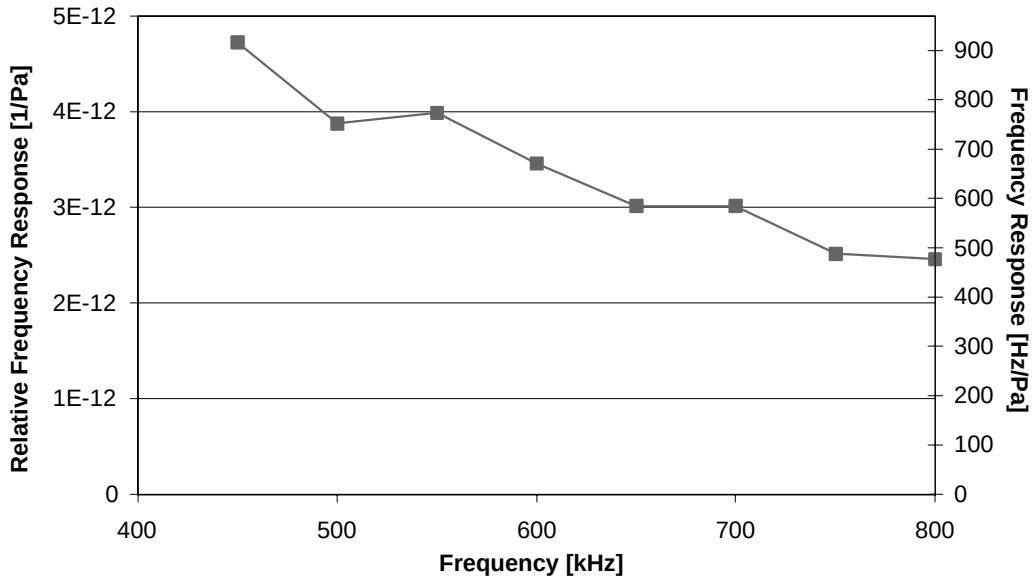

Figure 9.1. Relative and absolute frequency responsivity of the DFB fibre laser sensor.

long for high frequency acoustic sensing. DFB fibre lasers, [2] consisting of a single phase-shifted FBG written into a rare-earth doped fibre, should be very attractive for acoustic sensing owing to i) their robust single mode operation, ii) an extremely narrow linewidth (1-10kHz), providing low noise, and iii) a very short sensitive length [3].

We here demonstrate a DFB fibre laser used as a hydrophone for acoustic measurements in the frequency range of 0.1 to 1 MHz. The frequency response, directivity, and noise spectrum are measured.

9.2 Experimental results

A 5 cm-long erbium-doped, acrylate coated DFB fibre laser with 80 mm diameter and an optical linewidth of $\sim$ 10 kHz (produced by Ionas, Denmark) was placed in a large water tank with 1.1 m diameter, $\sim$ 65 cm from the acoustic source, made from a broad-band (0.1 - 2.2 MHz) 15 mm diameter PVDF-disk. The acoustic source emitted bursts of 30-40 sine-periods to allow gated detection without interference with reflections from the walls of the tank. The acoustic field was directed normally to the fibre laser axis. The source was calibrated up to 800 kHz, using a calibrated probe hydrophone. The fibre laser was remotely pumped by a 1480-nm diode laser through a WDM and the back-propagating fibre laser light was directed through the WDM and into an unbalanced (ΔL = 18 m) Mach-Zender interferometer with manual polarisa-

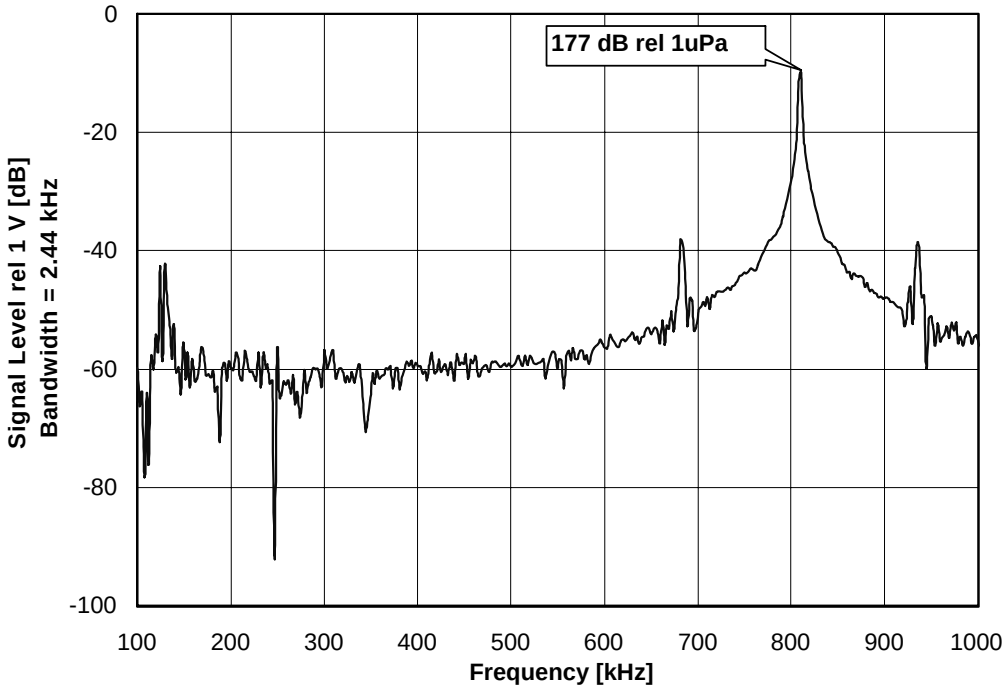

Figure 9.2. Output power spectrum of the sensor with an applied signal at 800kHz.

tion control and DC quadrature control by feedback to a piezo-electric fibre stretcher.

Fig. 9.1 shows the measured relative frequency response, $\Delta\nu/(\nu\delta P)$ and absolute frequency response $\Delta\nu/\Delta P$ of the DFB fibre laser acoustic sensor used as a hydrophone between 400 and 800 kHz, where ν is the laser frequency. The measurement is in good agreement with the expected relative frequency response of $\sim 4.5 \times 10^{-12}$ Pa^{-1} for a high frequency (axial constrained) optical fibre hydrophone [4]. The ~ 6 dB/octave roll-off in the frequency response can be due to a slight misalignment of acoustic wave-front relative to the fibre axis, as the width of the angular responsivity (see Fig. 9.4) is highly frequency dependent.

The output power spectrum of the sensor with an applied signal of 177 dB rel. 1 mPa at 800 kHz is shown in Fig. 9.2. From this we have derived a noise equivalent acoustic pressure of ~ 93 dB rel. 1 μPa/$\sqrt{\text{Hz}}$ (50 mPa/$\sqrt{\text{Hz}}$) at 800 kHz. This noise floor is determined by receiver noise, and can be reduced by 10-20 dB by optimising the electronic receiver and the receiver interferometer. The noise will then be determined by the fundamental thermal frequency noise of the fibre laser [1]. As seen in Fig. 9.2 the noise spectrum has a peak around 130 kHz (with a bandwidth of ~ 10 kHz), due to the laser relaxation oscillations, which is also causing side-band peaks around the signal at 800 ± 130 kHz.

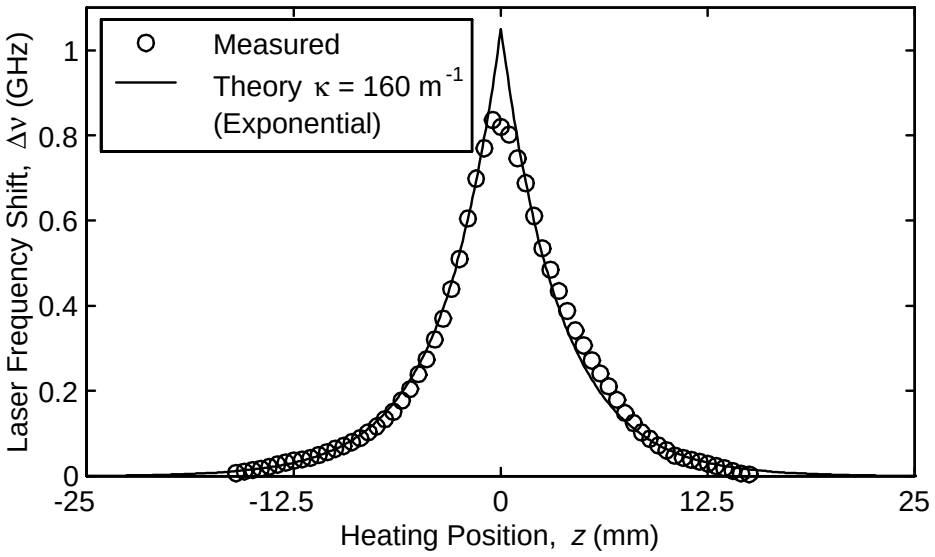

Figure 9.3. Spatial sensitivity dustribution of the fiber DFB laser measured with a heat perturbation technique.

The acoustic sensor is omnidirectional in the plane normal to the fibre axis owing to the symmetrical (cylindrical) shape of the fibre. When the acoustic wave is incident at an angle Φ relative to the fibre axis (as shown in the inset of Fig. 9.4) the response has an angular dependence, determined by the effective sensitive length (aperture) of the sensor.

Fig. 9.3 shows the spatial sensitivity distribution of the laser, measured by sacnning a heat source with an extension of about 1.5 mm over the laser fiber and measuring the resulting laser frequency shift. A good fit to the exponential distribution $\delta\nu \propto \exp(-2\kappa|z|)$ expected theoretically for an ideal discrete π phaseshifted DFB laser with grating strength $\kappa = 160$ m^{-1} is observed, except for is a rtelatively flat region close to $z = 0$. This flat region is attributed to the distributed nature of the grating phase-shift. The aperture, defined as the distance between the points where the sensitivity has dropped to 1/2 of its peak value, is 6.7 mm.

Fig. 9.4 shows the measured angular responsivity of the DFB fibre laser sensor at 800 kHz, which has a narrow central lobe with a 3-dB width of 6.4°. This width will decrease with increasing acoustic wavelength, which at 800 kHz is close to 2 mm. The angular responsitivity expected from the spatial characterization measeurements, calculated by taking a Fourier transform of the measurements in Fig. 9.3, is also shown i n the figure, along with a Lorenzian curve corresponding to the ideal theoretical curve in Fig. 9.3. The central lobe of the angular measurements is similar to the calculated curves.

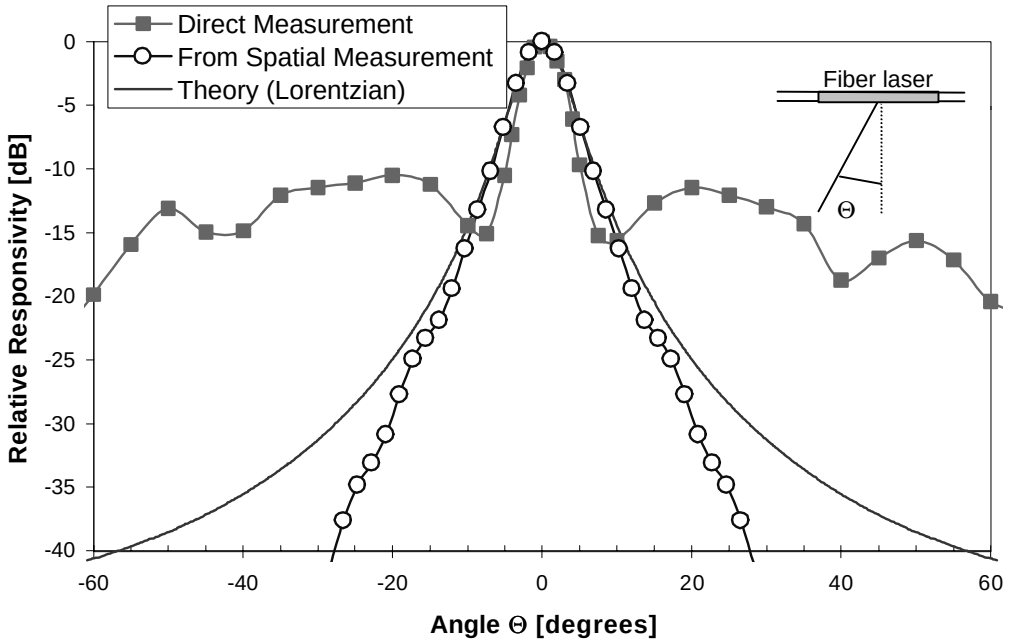

Figure 9.4. Measured and calculated angular responsivity at 800kHz. The calculations are based on the measured spatial sensitivity distribution along the fibre laser.

The side-bands in the direct angular measurements may be due to unresolved grating imperfections with high spatial frequencies (which would not be resolved by the spatial measurements), coating effects or air bubbles on the fibre.

9.3 Summary

We demonstrate for the first time a DFB fibre laser used as a hydrophone. The pressure sensitivity of the laser frequency ranges from 1 to 0.5 kHz/Pa between 400 and 800 kHz. The noise equivalent pressure was ~ 93 dB rel. 1 μPa/$\sqrt{\text{Hz}}$. The angular responsivity at 800 kHz had a central lobe with a 3-dB width of 6.4°, corresponding to an effective sensitive length of approximately 6mm, which is much shorter than the laser cavity length of 5 cm.

References

[1] Koo, K.P., and Kersey, A.D., "Bragg grating-based laser sensors systems with interferometric interrogation and wavelength division multiplexing," J. Lightwave Technol., Vol. 13, pp. 1243-1249, 1995.

[2] Kringlebotn, J.T., Archambault, J.-L., Reekie, L., and Payne, D., "Er^{3+}:Yb^{3+}-codoped fiber distributed-feedback laser," Opt. Lett., Vol. 19, pp. 2101-2103, 1994.

[3] Rønnekleiv, E., Ibsen, M., Zervas, M.N., and Laming, R.I., "Characterisation of fiber DFB lasers via an index perturbation method," to be published in Appl. Opt., Vol.38, No. 21, (20. July) 1999.

[4] Culshaw, B., Davies, D.E.N., and Kingsley, S.A., "Acoustic sensitivity of optical fibre waveguides," Electron. Lett., Vol. 13, pp. 760-761, 1977.